Research Article J. Electrochem. Sci. Technol., 2023, 14(3), 243-251

Ni Foam-Supported Ni Nanoclusters for Enhanced Electrocatalytic Oxygen Evolution Reaction

Hoeun Seong[1†], Jinhee Kim[1†], Kiyoung Chang[1], Hyun-woo Kim[1], Woojun Choi[2], and Dongil Lee[1*]
[1]Department of Chemistry, Yonsei University, Seoul 03722, Republic of Korea
[2]Department of Chemistry and Medical Chemistry, Yonsei University, Wonju, Gangwon 26493, Republic of Korea

ABSTRACT

Developing oxygen evolution reaction (OER) electrocatalysts is essential to accomplish viable CO_2 and water electrolysis. Herein, we report the fabrication and OER performance of Ni-foam (NF)-immobilized Ni_6 nanoclusters (NCs) (Ni_6/NF) prepared by a dip-coating process. The Ni_6/NF electrode exhibited a high current density of 500 mA/cm^2 for the OER at an overpotential as low as 0.39 V. Ni_6/NF exhibited high durability in an alkaline solution without corrosion. Electrokinetic studies revealed that OER can be easily initiated on Ni_6 NC with fast electron-transfer rates. Finally, we demonstrated stable CO_2-to-CO electroreduction using an NC-based zero-gap CO_2 electrolyzer operated at a current density of 100 mA/cm^2 and a full-cell potential of 2.0 V for 12 h.

Keywords : Oxygen evolution reaction, CO_2 reduction reaction, Nickel, Nanocluster, Electrode

Received : 13 January 2023, Accepted : 7 March 2023

1. Introduction

Electrochemical CO_2 reduction reaction (CO_2RR) and hydrogen evolution reaction (HER) are recognized as promising strategies for storing renewable energy as chemical feedstock [1,2]. However, practical applications of CO_2RR and water electrolysis have suffered from the anodic oxygen evolution reaction (OER) [3-5], which requires a high overpotential because of the kinetically slow four-coupled electron and proton transfer pathways. Several OER electrocatalysts have been developed to reduce the overpotential. In particular, precious-metal-based Ir or Ru catalysts are predominantly used at present [6]. Therefore, inexpensive electrocatalysts with high activity are extensively studied to realize economically feasible energy-conversion electrolysis.

Recently, transition-metal-based OER catalysts such as metal oxides, metal sulfides, and layered double hydroxides have been reported [7-9]. Among these, naturally abundant Ni catalysts have received considerable attention [10,11]. However, Ni catalysts generally undergo changes concerning the charge state and atomic structure during electrocatalysis [12,13]; therefore, correlating the catalytic activities with their structures is challenging. In addition, cutting-edge Ni-based OER catalysts typically require thermal treatment, significantly increasing the cost of production [14-16].

Recently, atomically precise metal nanoclusters (NCs) have been studied in various electrochemical systems [17-23]. They can be isolated as single species with molecular purity and show well-defined structures, as confirmed by X-ray crystallography [24]. Among them, Ni NCs are typically synthesized in the formula $Ni_n(SR)_{2n}$, where SR is a thiolate ligand (abbreviated as Ni_n) [25-27]. The Ni NCs are stable because of ligand protection and delocalized electrons on the cyclic ring structure [28,29]. In previous studies, Ni NCs have been exploited as OER electrocatalysts, typically immobilized on carbon substrates [30-33]. Kauffman *et al.* reported that Ni_6 NC exhibits higher activity than Ir or NiO. Using density functional theory calculations, they ascribed the high OER activity of the Ni_6 NC to the enhanced kinetics in the first electron transfer step [30]. Hus-

†These authors contributed equally to this work.
*E-mail address: dongil@yonsei.ac.kr

DOI: https://doi.org/10.33961/jecst.2023.00024

sain *et al.* also reported the OER activities of Ni_4 and Ni_6 NCs, which exhibited higher OER activities than typical Ni-based electrodes [31]. Recently, Jin *et al.* reported the size-dependent OER activities of Ni_4, Ni_5, and Ni_6 NCs [32].

Although Ni NCs have been extensively studied as efficient electrocatalysts for water oxidation, their OER activity is far below the commercially viable level. Although carbon supports offer high electronic conductivity, they are prone to corrosion under electrochemical oxidation [34,35]. Although graphitized carbon species show relatively slow corrosion rates compared with typical carbon black [36], they also gradually corrode at high anodic potentials during long-term operations. Therefore, carbon-free OER catalysts with high durability are in high demand.

This study reports the preparation and OER activity of Ni-foam (NF)-supported Ni_6 NCs (Ni_6/NF) fabricated using the dip-coating method. The Ni_6 NC exhibited extraordinary OER activity on an NF substrate in an alkaline electrolyte. It showed high OER activity with a current density (j) of 500 mA/cm^2 at a low overpotential (η) of 0.39 V, outperforming the commercial IrO_2 electrocatalysts. Electrokinetic studies revealed that the high OER activity of Ni_6/NF originates from facile electron transfer on the non-corrosive substrate. In this study, an NC-based zero-gap CO_2 electrolyzer was constructed using a Au_{25}-immobilized gas diffusion electrode (Au_{25}/GDE) and Ni_6/NF electrodes as the cathode and anode, respectively, which exhibited highly active and stable CO_2RR and OER operations.

2. Experimental

2.1 NC Synthesis

The $Ni_6(SEtPh)_{12}$ NCs were synthesized following a previously reported method [37]. Briefly, $NiCl_2{\cdot}6H_2O$ (Merck, reagent grade, 0.42 mmol) and tetraoctylammonium bromide (Merck, 98%, 0.89 mmol) were dissolved in tetrahydrofuran (100 mL). After stirring for 30 min, 2-phenylethanethiol (HSEtPh) (Merck, 98%, 2.17 mmol) was added. $NaBH_4$ (Merck, 99%, 4.23 mmol) dissolved in cold water (14 mL) was added after 5 min, and the solution was stirred for an additional 24 h. The product was evaporated using a rotary evaporator. The organic phase was then separated and washed several times with methanol. The product was extracted using dichloromethane (CH_2Cl_2) and crystallized by layering ethanol (10 mL) over the NC solution in CH_2Cl_2 (10 mL).

$Au_{25}(SC_6H_{13})_{18}$ NC was prepared according to the previously reported procedure [38].

2.2 Characterizations of NCs

Ultraviolet-visible (UV-vis) absorption spectra of the NCs in CH_2Cl_2 were obtained using a Shimadzu UV-vis-NIR spectrophotometer (UV-3600). Electrospray ionization (ESI) mass spectra were acquired using the negative ion mode in an ESI mass spectrometer (Agilent 6230 TOF LC/MS).

Single-crystal X-ray diffraction (SC-XRD) analysis was conducted on the crystals of $Ni_6(SEtPh)_{12}$ NCs grown at 25°C by layering hexanes over CH_2Cl_2 solution of $Ni_6(SEtPh)_{12}$ NCs (Fig. S1). The PAL BL2DSMDC program [39] was used for data collection. Cell refinement, reduction, and absorption correction were performed using HKL3000sm (Version 716.7) [40]. The crystal structure of $Ni_6(SEtPh)_{12}$ NCs was solved using the direct method with SHELX-XT (Ver. 2014/5) [41] and refined by full-matrix least-squares calculations with the SHELX-XL (Ver. 2016/4) [42] in the Olex2 [43] program package. The diffused electrons in large solvent-accessible void were treated using the SQUEEZE procedure (PLATON) [44,45].

After electrolysis experiments, the Ni_6 NCs and Nafion were extracted from the Ni_6/NF electrode using a mixture of CH_2Cl_2 and methanol. Pure Ni_6 NCs were further extracted with CH_2Cl_2 with approximately 50% of the recovery. The recovered NCs were analyzed using UV-vis absorption spectroscopy and mass spectrometry (Bruker, Autoflex Max).

2.3 Preparation and Characterization of Electrodes

The Ni_6 suspension for the 1 cm^2-electrode was prepared by mixing Ni_6 NC (1.0 mg) and Nafion (10 μL) (5 wt.%, Merck) in methanol (1.0 mL) and sonicating for 10 min. For large-scale fabrication, the suspension was scaled up proportionally to the electrode area. The Ni_6/NFs were prepared by dipping the NF (29-04275-01, Invisible Inc.) in the prepared suspension for 5 s and drying it for 1 h under a dynamic vacuum. We determined the loading amount of Ni_6 NC on the NF by measuring the weight change of the NF after the dipping process. Typical NC loading was determined to be 0.089±0.008 mg/cm^2. In addition, the loading amount was controllable (0.02, 0.05,

and 0.1 mg/cm^2) by changing the Ni_6 concentration (0.2–1.0 mg/mL) in the dipping solution. Scanning electron microscopy (SEM), and energy-dispersive X-ray spectroscopy (EDS) analyses of the Ni_6/NF electrodes were performed using a JEOL scanning electron microscope (JEOL-7800F). For the EDS analysis of sulfur of the Ni_6/NF electrodes, the same weight of polyvinylidene fluoride (PVDF) binder was used instead of the sulfur-containing Nafion. The Ni_6-immobilized GDE (W1S1011, Ce-Tech) (Ni_6/GDE) was fabricated by spreading Ni_6 NC solution (0.5 mg of Ni_6 NC in 0.16 mL of acetone and 0.16 mL of CH_2Cl_2) on the microporous layer of 1 cm^2-GDE. To compare the OER activities, commercial IrO_2-coated GDEs (IrO_2/GDEs) were purchased from Dioxide Materials.

The Au_{25}/GDE was prepared according to the procedure reported in a previous study [19].

2.4 Electrochemical Measurements

The half-cell measurement of the electrochemical OER was conducted using a three-electrode system in a one-compartment cell containing 20 mL of 1.0 M KOH solution with vigorous stirring to remove the generated O_2 bubbles and promote mass transport. The prepared anodes were used as the working electrodes; the typical anode area was 1 cm^2. A Pt foil cathode (1 cm^2) and Ag/AgCl (1.0 M KCl) were employed as the counter and reference electrodes, respectively.

Linear sweep voltammetry (LSV), chronopotentiometry (CP), and electrochemical impedance spectroscopy (EIS) measurements were performed using a potentiostat (ZIVE BP2, WonATech). The NF anodes were pre-activated by conducting CP at 100 mA for 2 h before measuring their OER activity. LSV was conducted at a scan rate of 20 mV/s. The impedance spectra were recorded in a potentiostatic mode at various applied potentials in the frequency range of 100 kHz to 0.01 Hz with an amplitude of 10.0 mV.

The anode potentials recorded on the Ag/AgCl scale ($E_{Ag/AgCl}$) were converted to the reversible hydrogen electrode (RHE) scale (E_{RHE}) and η using the following equations:

$$E_{RHE} = E_{Ag/AgCl} + 0.21 + 0.059\ pH \quad (1)$$

$$\eta = E_{RHE} - 1.23\ V \quad (2)$$

The potential (E) was iR-compensated.

To measure the Faradaic efficiency of O_2 (FE_{O_2}), a laboratory-made, gas-tightened H-cell was used [20]. Residual air was purged with Ar gas, and the cell was tightly sealed. CP was performed at 50 mA for 1 h. After electrolysis, the headspace of the anode was analyzed by gas chromatography (GC) (GC 7890B, Agilent) equipped with a thermal conductivity detector and a flame ionization detector.

The full-cell measurement for CO_2RR-OER co-electrolysis was conducted in a zero-gap CO_2 electrolyzer [46], and the active areas of the cathode and anode were confined to 5 cm^2 by a flow field. CO_2 gas (200 sccm, humidified at 25°C) was fed into the cathode flow field, and fresh 1.0 M KOH was supplied to the anode line. In all CO_2RR experiments, CO and H_2 were produced as cathodic reaction products.

3. Results and Discussion

$Ni_6(SEtPh)_{12}$ NC was prepared according to a previously report (see the Experimental section for details) [37]. The Ni_6 NC was synthesized as a single species (Fig. 1a) with a yield of ~50% based on Ni. The SC-XRD analysis clearly revealed the atomic structure of the $Ni_6(SEtPh)_{12}$ NC, which is composed of six hexagonally arranged Ni atoms and twelve thiolate ligands located at intervals of the Ni ring (Fig. 1b). The atomic structure is consistent with that reported previously [37]. The Ni_6 NC showed exceptional stability owing to its protecting ligands and electron delocalization following the ring structure [28,29].

The synthesized Ni_6 NCs were further characterized using ESI mass spectrometry and UV-vis absorption spectroscopy. The single peak in the ESI mass spectrum (Fig. 1c) indicates that the obtained NC exists with molecular purity. The peak observed at m/z of 2034 Da was assigned to the NC-chloride adduct of $[Ni_6(SEtPh)_{12}]Cl^-$ formed during ionization, by matching the simulated isotope pattern (Fig. 1c, inset). The UV-vis absorption spectrum of the Ni_6 NC (Fig. 1d) exhibits four characteristic absorption peaks at 339, 410, and 535 nm, indicating that the Ni_6 NC has a discrete energy level.

The Ni_6 NCs are very small (*ca.* 1.6 nm in diameter, including the ligand chain) and stable; therefore, they can be directly immobilized on NF electrodes

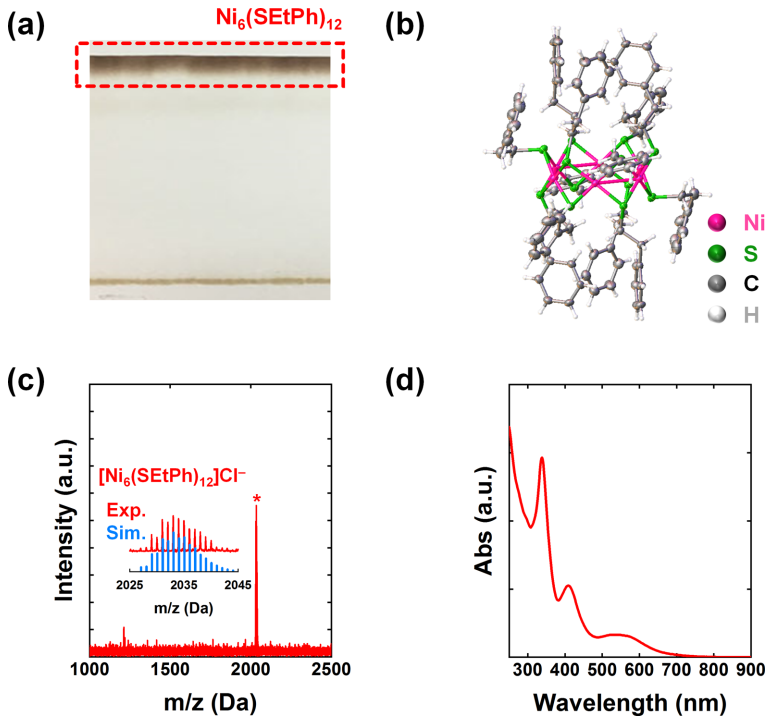

Fig. 1. (a) Digital photograph of the preparative thin layer chromatography separation of the Ni_6 NC products. (b) Crystal structure of the $Ni_6(SEtPh)_{12}$ NC. (c) Negative-mode ESI mass and (d) UV-vis absorption spectrum of the $Ni_6(SEtPh)_{12}$ NC. The inset in (c) compares the experimental data (red) and the simulated isotope patterns (blue).

even without support such as carbon black. The dip-coating process is considered an easily processable catalyst coating method [47,48]. Ni_6/NF was prepared by simply dipping the NF into a Ni_6 dipping solution (Fig. 2a). Methanol, in which the Ni_6 NC is poorly soluble, was chosen as the suspension medium to make Ni_6 NC weakly interact with the solvent and thereby anchor on NF. The use of a binder, either PVDF or Nafion, assisted the dispersion of the Ni_6 NCs (Fig. S2), resulting in a uniform suspension. Despite short dipping time, the loading amount was found to be consistent in the reproducible test (Fig. S3).

To confirm the distribution of Ni_6 NCs on the NF, we performed the SEM and corresponding EDS of the Ni_6/NF. The existence of the Ni_6 NC can be tracked by the sulfur atoms of the thiolate ligands in the EDS elemental mapping image. Therefore, we used PVDF as a binder instead of Nafion for the SEM-EDS measurements to avoid interference from sulfur of Nafion. SEM images show some aggregates of Ni_6 NCs on the NF substrate (Figs. 2b and S4a). However, the SEM-EDS elemental mapping images of Ni_6/NF show that the Ni_6 NCs were uniformly distributed throughout the NF, as monitored by the sulfur atoms (Figs. 2b and S5).

The OER activity of Ni_6/NF was measured by LSV in a 1.0 M KOH electrolyte solution. Before measuring the OER activity, the electrodes were pretreated by conducting CP at an anodic current of 100 mA/cm^2 for 2 h. A significant increase in the oxidative current was observed after CP (Fig. S6a), suggesting that Ni_6/NF underwent some kind of activation process during CP. After CP electrolysis, Ni_6/NF displayed a clean surface without NC aggregates (Fig. S4b). Extracting NCs from Ni_6/NF after electrolysis, the electrode exhibited OER activity similar to that of bare NF (Fig. S6b), and the retrieved NCs showed nearly identical profiles to the intact NCs (Fig. S7). These results suggest that the activation can be attributed to the uniform spreading of Ni_6 NCs on the NF substrate during CP electrolysis.

As shown in Fig. 2c, Ni_6/NF showed a higher OER activity than bare NF. The OER current on Ni_6/NF

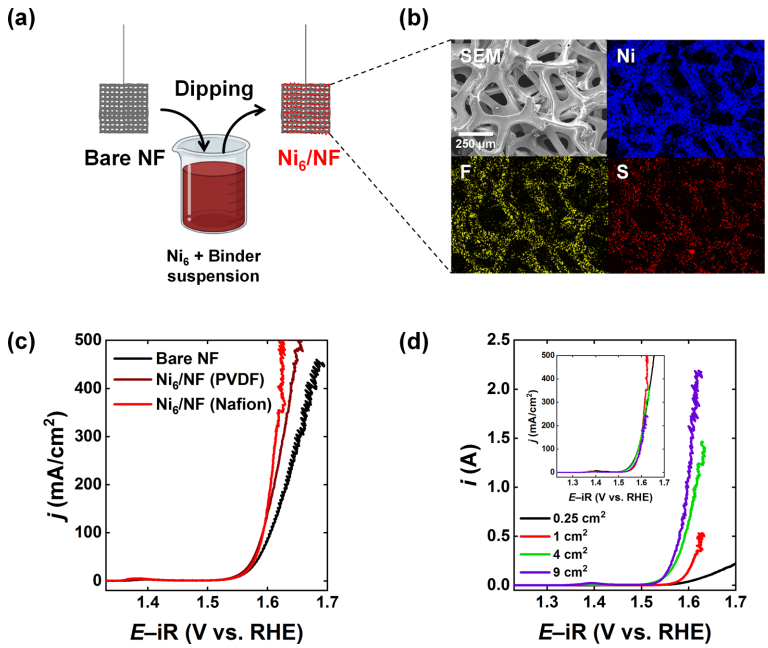

Fig. 2. (a) Scheme describing the dip-coating process of Ni_6 NCs onto NF. (b) SEM and SEM-EDS elemental mapping images of Ni_6/NF fabricated with PVDF binder. LSV curves recorded (c) on bare NF, Ni_6/NF (PVDF), and Ni_6/NF (Nafion) electrodes, and (d) on various sized Ni_6/NF (Nafion) electrodes.

started from an η of 0.30 V and reached 500 mA/cm^2 at a low η of 0.39 V. The OER activity of Ni_6/NF was slightly higher with the Nafion binder than with the PVDF binder because of the enhanced ion conductivity of the electrode [49]. Thus, OER experiments were conducted on Ni_6/NF with a Nafion binder. The OER activity of Ni_6/NF increased with increasing Ni_6 loading (Fig. S8a), showing the highest activity at a loading of 0.1 mg/cm^2. Both η values for achieving 10 and 100 mA/cm^2 were decreased as increasing the loading amount (Fig. S8b).

The high processability of the dipping method enables large-scale preparation of Ni_6/NF. Fig. 2d shows the OER activity of various sized Ni_6/NF. Evidently, the total oxidative current increases with increasing electrode area. The dip-processed 9 cm^2 of Ni_6/NF shows an OER current of 2.0 A at an η of 0.38 V. Normalized to the area, the *j*-*E* profile of the electrodes was nearly identical (Fig. 2d, inset), indicating that the unit activity is similar for different-sized electrodes. This suggests that large-area Ni_6/NF electrodes can be readily fabricated by scaling up the dipping process.

Though Ni NCs have been exploited as OER electrocatalysts in previous reports [30-32], they were supported by carbon substrates. However, carbonaceous materials easily corrode under electro-oxidation conditions [34]. Therefore, Ni_6/NF is a promising electrode for sustainable OER. To compare the effect of the carbon substrate, a carbon-based GDE was used as the substrate for the Ni_6 and IrO_2 catalysts. IrO_2/GDE exhibited a lower η (0.27 V) for the onset of the catalytic current than Ni_6/NF; however, its OER activity was lower than that of Ni_6/NF over 100 mA/cm^2 (Fig. 3a). Surprisingly, Ni_6/GDE showed extremely low catalytic activity compared to Ni_6/NF and IrO_2/GDE (Fig. 3a). The OER activity obtained for Ni_6/GDE was in a similar range to those obtained in other studies [30-33].

To investigate the origin of the difference in OER activities, we quantitatively measured the FE_{O_2} on the electrodes (Fig. 3b) using GC analysis. IrO_2/GDE produced a FE_{O_2} of 98% despite using a carbon substrate. This is attributed to the high loading (4.8 mg) of the IrO_2 catalyst, which can prevent the electro-oxidation of GDE. However, the FE_{O_2} measured for Ni_6/GDE was significantly low (82%), indicating that the GDE was actively corroded during electrochemi-

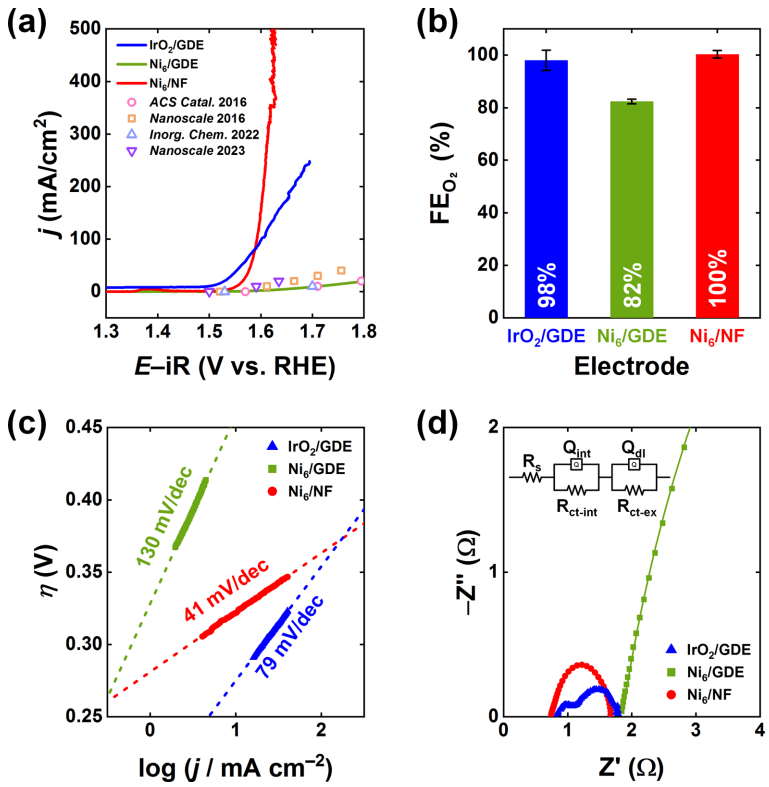

Fig. 3. (a) LSV curves, (b) FE for O_2 production at current density of 50 mA/cm^2, (c) Tafel, and (d) Nyquist plots at 1.64 V *vs.* RHE measured on Ni_6/NF (0.1 mg of catalyst), Ni_6/GDE (0.5 mg), and IrO_2/GDE (4.8 mg) in 1.0 M KOH solution. The current densities obtained on Ni_6 NCs in other reports are shown for comparison in (a). The equivalent electrical circuit [55] used to obtain the impedance parameters is shown in the inset of (d), where R_s, $R_{ct\text{-}int}$, and $R_{ct\text{-}ex}$ denote the solution, internal and external charge transfer resistances, respectively, and Q_{int} and Q_{dl} are the constant phase element representing the internal and double layer capacitance.

cal OER (Fig. S9). In contrast, Ni_6/NF only performs OER with FE_{O_2} of 100%, indicating that all the produced electrons originate from water oxidation without any side reactions. This result suggests that corrosion-free electrodes can lead to highly active OER activities.

To further investigate the origin of the high OER activity of Ni_6/NF, electrokinetic studies were performed. First, Tafel analysis was performed by plotting log j *vs.* η in the kinetically controlled region. In Fig. 3c, IrO_2/GDE shows a Tafel slope of 79 mV/dec, which is consistent with the reported values [50-52]. The Tafel slope obtained for Ni_6/GDE is high (130 mV/dec) owing to carbon degradation. In contrast, the slope of Ni_6/NF was very low at 41 mV/dec, indicating that Ni_6/NF can initiate the OER with fast kinetics. In particular, the OER in a neutral-alkaline solution involves four concerted proton-electron transfers described by the following elementary steps (here, * indicates the active site) [53]:

$$* + OH^- \rightarrow *OH + e^- \quad (3)$$

$$*OH + OH^- \rightarrow *O + H_2O + e^- \quad (4)$$

$$*O + OH^- \rightarrow *OOH + e^- \quad (5)$$

$$*OOH + OH^- \rightarrow * + O_2 + H_2O + e^- \quad (6)$$

The theoretical Tafel slopes were 120 and 40 mV/dec when steps (3) and (4) were the rate-determining steps (RDSs), respectively [54]. Thus, the low Tafel slope of ~40 mV/dec observed for Ni_6 NC suggests that step (4) is the RDS of the OER on the Ni_6/NF

electrode. This implies that the first hydroxide adsorption is facilitated on the Ni_6/NF with fast electron transfer. This result is in good agreement with previously reported theoretical predictions for the OER on Ni_6 NC [30].

EIS was performed to compare the electron transfer kinetics of the electrodes. Fig. 3d shows the Nyquist plots obtained on IrO_2/GDE, Ni_6/GDE, and Ni_6/NF at 1.64 V in 1.0 M KOH. IrO_2/GDE shows two semicircles; the small semicircle in the high-frequency region represents the internal charge transfer of the electrode ($R_{ct\text{-}int}$), and the second semicircle in the low-frequency region is accompanied by external charge transfer between the electrode and reactants ($R_{ct\text{-}ex}$) [55]. $R_{ct\text{-}int}$ was absent on the Ni_6/GDE and Ni_6/NF electrodes. The electron transfer rate constant (k_{ET}) [56] extracted from the sum of ($R_{ct\text{-}int}$+$R_{ct\text{-}ex}$) is shown in Fig. S10. Ni_6/NF exhibits the largest k_{ET} magnitude compared to IrO_2/GDE and Ni_6/GDE, indicating that electron transfer from the reactants to Ni_6/NF is facile. These electrokinetic results strongly corroborate the extraordinary OER activity of Ni_6/NF.

To evaluate the feasibility of Ni_6/NF in CO_2 electrolysis, the Ni_6/NF anode was coupled with a Au_{25}/GDE cathode in a zero-gap CO_2 electrolyzer (see the Experimental Section for details). Ni_6/NF exhibits higher cell activity than that of the IrO_2/GDE (Fig. 4a). The cell potential obtained using the Ni_6/NF anode was approximately 0.4 V smaller than that of IrO_2/GDE at a current density of 100 mA/cm^2. We performed CP experiments and GC analyses to confirm the origin of the cathodic currents. Fig. 4b shows the partial current densities and selectivities for CO and H_2 measured using the zero-gap CO_2 electrolyzer. Regardless of the anodes, Au_{25}/GDE exhibits high selectivity for CO production; however, the cell potentials were reduced by more than 0.4 V with Ni_6/NF due to reduced OER overpotentials. Furthermore, a long-term stability test of Ni_6/NF was conducted at 100 mA/cm^2 (Fig. 4c). During the initial

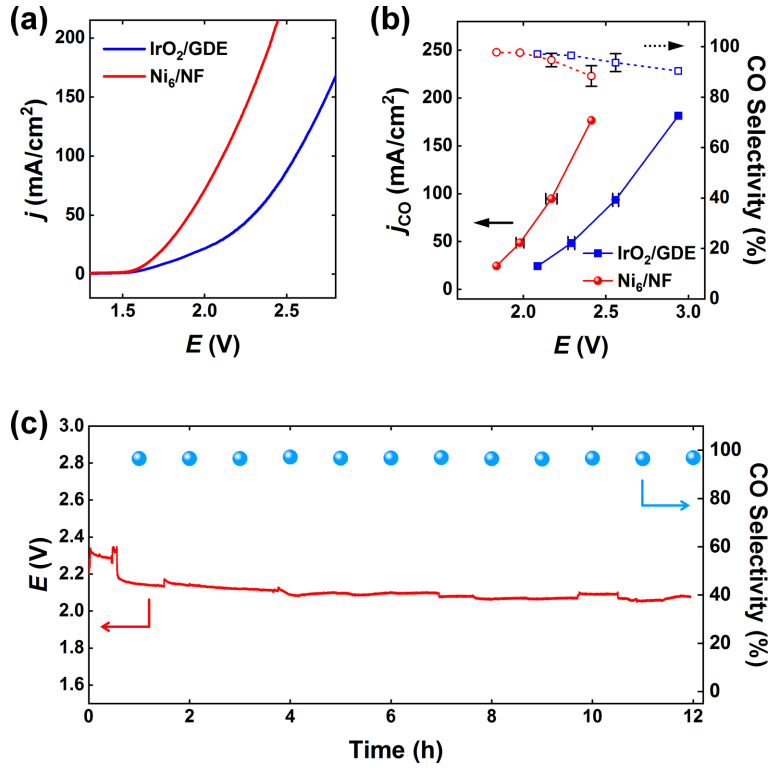

Fig. 4. (a) LSV curves, (b) j_{CO}, and CO selectivity measured on IrO_2/GDE and Ni_6/NF anodes in zero-gap CO_2 electrolyzer. Au_{25}/GDE (0.08 mg/cm^2) was used as cathode. (c) Long-term CO_2 electrolysis of Au_{25}/GDE-Ni_6/NF equipped zero-gap CO_2 electrolyzer monitored by cell potential and CO selectivity at 100 mA/cm^2.

operation (~2 h), the cell potential gradually decreased owing to the activation of the electrodes. The electrolyzer then sustained its reactions at a cell potential of ~2.0 V for 12 h, maintaining a CO selectivity above 95%. The energy efficiency of CO_2-to-CO conversion at 100 mA/cm^2 is above 63%, which is higher than those reported for the most efficient electrocatalysts to the best of our knowledge [57-60].

4. Conclusions

We demonstrated that the dip-processed Ni_6/NF electrode exhibits exceptional OER activity in alkaline media. The Ni_6/NF electrode was fabricated by simply dipping NF into the NC suspension. The Ni_6/NF electrode showed higher OER activity than those of IrO_2/GDE and Ni_6/GDE without corrosion under oxidative conditions. Tafel analysis and EIS revealed that fast electron transfer on Ni_6/NF resulted in enhanced kinetics during the OER. The zero-gap CO_2 electrolyzer with the Ni_6/NF anode was stably operated at a current density of 100 mA/cm^2 for 12 h while maintaining a cell potential of ~2.0 V and CO selectivity above 95%. This study provides a useful methodology for the facile and uniform preparation of NC-catalyst-coated electrodes.

Acknowledgment

This work was supported by the Carbon-to-X Project (Project No. 2020M3H7A1096388) through the NRF, funded by the Korea government (MSIT) and the Korea Electric Power Corporation (grant No. R20XO02-23).

Supporting Information

Supporting Information is available at https://doi.org/10.33961/jecst.2023.00024

References

[1] M. S. Dresselhaus and I. L. Thomas, *Nature*, **2001**, *414*, 332-337.
[2] P. De Luna, C. Hahn, D. Higgins, S. A. Jaffer, T. F. Jaramillo and E. H. Sargent, *Science*, **2019**, *364*, eaav3506.
[3] W. H. Lee, H. N. Nong, C. H. Choi, K. H. Chae, Y. J. Hwang, B. K. Min, P. Strasser and H.-S. Oh, *Appl. Catal. B*, **2020**, *269*, 118820.
[4] E. Fabbri and T. J. Schmidt, *ACS Catal.*, **2018**, *8(10)*, 9765-9774.
[5] A. K. Niaz and H.-T. Lim, *J. Electrochem. Sci. Technol.*, **2022**, *13(3)*, 369-376.
[6] Y. Lee, J. Suntivich, K. J. May, E. E. Perry and Y. Shao-Horn, *J. Phys. Chem. Lett.*, **2012**, *3(3)*, 399-404.
[7] T. Reier, Z. Pawolek, S. Cherevko, M. Bruns, T. Jones, D. Teschner, S. Selve, A. Bergmann, H. N. Nong, R. Schlögl, K. J. J. Mayrhofer and P. Strasser, *J. Am. Chem. Soc.*, **2015**, *137(40)*, 13031-13040.
[8] Z. Chen, M. Ju, M. Sun, L. Jin, R. Cai, Z. Wang, L. Dong, L. Peng, X. Long, B. Huang and S. Yang, *Angew. Chem. Int. Ed.*, **2021**, *60(17)*, 9699-9705.
[9] P. Chauhan and B. Lal, *J. Electrochem. Sci. Technol.*, **2022**, *13(4)*, 497-503.
[10] L.-F. Li, Y.-F. Li and Z.-P. Liu, *ACS Catal.* **2020**, *10(4)*, 2581-2590.
[11] T. Kou, S. Wang, J. L. Hauser, M. Chen, S. R. J. Oliver, Y. Ye, J. Guo and Y. Li, *ACS Energy Lett.*, **2019**, *4(3)*, 622-628.
[12] C. Cui, L. Gan, M. Heggen, S. Rudi and P. Strasser, *Nature Mater.*, **2013**, *12*, 765-771.
[13] J. Huang, N. Hörmann, E. Oveisi, A. Loiudice, G. L. De Gregorio, O. Andreussi, N. Marzari and R. Buonsanti, *Nat. Commun.*, **2018**, *9*, 3117.
[14] D. Wang, Q. Li, C. Han, Q. Lu, Z. Xing and X. Yang, *Nat. Commun.*, **2019**, *10*, 3899.
[15] Z. Cai, L. Li, Y. Zhang, Z. Yang, J. Yang, Y. Guo and L. Guo, *Angew. Chem. Int. Ed.*, **2019**, *58(13)*, 4189-4194.
[16] F. Qin, Z. Zhao, M. K. Alam, Y. Ni, F. Robles-Hernandez, L. Yu, S. Chen, Z. Ren, Z. Wang and J. Bao, *ACS Energy Lett.*, **2018**, *3(3)*, 546-554.
[17] K. Kwak, U. P. Azad, W. Choi, K. Pyo, M. Jang and D. Lee, *ChemElectroChem*, **2016**, *3(8)*, 1253-1260.
[18] K. Kwak, W. Choi, Q. Tang, M. Kim, Y. Lee, D. Jiang and D. Lee, *Nat. Commun.*, **2017**, *8*, 14723.
[19] H. Seong, V. Efremov, G. Park, H. Kim, J. S. Yoo and D. Lee, *Angew. Chem. Int. Ed.*, **2021**, *60(26)*, 14563-14570.
[20] W. Choi, H. Seong, V. Efremov, Y. Lee, S. Im, D.-H. Lim, J. S. Yoo and D. Lee, *J. Chem. Phys.*, **2021**, *155*, 014305.
[21] M. Kim, Q. Tang, A. V. Narendra Kumar, K. Kwak, W. Choi, D. Jiang and D. Lee, *J. Phys. Chem. Lett.*, **2018**, *9(5)*, 982-989.
[22] V. D. Thanthirige, M. Kim, W. Choi, K. Kwak, D. Lee and G. Ramakrishna, *J. Phys. Chem. C*, **2016**, *120(40)*, 23180-23188.
[23] D. C. Lim, J. H. Jeong, K. Hong, S. Nho, J.-Y. Lee, Q. V. Hoang, S. K. Lee, K. Pyo, D. Lee and S. Cho, *Prog. Photovolt.*, **2018**, *26(3)*, 188-195.
[24] R. Jin, C. Zeng, M. Zhou and Y. Chen, *Chem. Rev.*, **2016**, *116(18)*, 10346-10413.
[25] P. Woodward, L. F. Dahl, E. W. Abel and B. C. Crosse, *J. Am. Chem. Soc.*, **1965**, *87(22)*, 5251-5253.
[26] C. Zhang, T. Matsumoto, M. Samoc, S. Petrie, S. Meng,

T. Christopher Corkery, R. Stranger, J. Zhang, M. G. Humphrey and K. Tatsumi, *Angew. Chem. Int. Ed.*, **2010**, *49(25)*, 4209-4212.
[27] W. Zhang, J. Hong, J. Zheng, Z. Huang, J. Zhou and R. Xu, *J. Am. Chem. Soc.*, **2011**, *133(51)*, 20680-20683.
[28] A. Datta, N. S. John, G. U. Kulkarni and S. K. Pati, *J. Phys. Chem. A*, **2005**, *109(51)*, 11647-11649.
[29] A. Muñoz-Castro, *J. Phys. Chem. A*, **2011**, *115(39)*, 10789-10794.
[30] D. R. Kauffman, D. Alfonso, D. N. Tafen, J. Lekse, C. Wang, X. Deng, J. Lee, H. Jang, J. Lee, S. Kumar and C. Matranga, *ACS Catal.*, **2016**, *6(2)*, 1225-1234.
[31] K. S. Joya, L. Sinatra, L. G. AbdulHalim, C. P. Joshi, M. N. Hedhili, O. M. Bakr and I. Hussain, *Nanoscale*, **2016**, *8*, 9695-9703.
[32] S. Srinivasan, Z. Liu, S. House and R. Jin, *Inorg. Chem.*, **2023**, *62(5)*, 1875-1884.
[33] S. Funaki, T. Kawawaki, T. Okada, K. Takemae, S. Hossain, Y. Niihori, T. Naito, M. Takagi, T. Shimazaki, S. Kikkawa, S. Yamazoe, M. Tachikawa and Y. Negishi, *Nanoscale*, **2023**, *15*, 5201-5208.
[34] S. Möller, S. Barwe, J. Masa, D. Wintrich, S. Seisel, H. Baltruschat and W. Schuhmann, *Angew. Chem. Int. Ed.*, **2020**, *59(4)*, 1585-1589.
[35] Y. Yi, G. Weinberg, M. Prenzel, M. Greiner, S. Heumann, S. Becker and R. Schlögl, *Catal. Today*, **2017**, *295*, 32-40.
[36] Y. Sato, N. Yamada, S. Kitano, D. Kowalski, Y. Aoki and H. Habazaki, *J. Mater. Chem. A*, **2022**, *10*, 8208-8217.
[37] H. N. Kagalwala, E. Gottlieb, G. Li, T. Li, R. Jin and S. Bernhard, *Inorg. Chem.*, **2013**, *52(15)*, 9094-9101.
[38] B. Kim, H. Seong, J. T. Song, K. Kwak, H. Song, Y. C. Tan, G. Park, D. Lee and J. Oh, *ACS Energy Lett.*, **2020**, *5(3)*, 749-757.
[39] J. W. Shin, K. Eom and D. Moon, *J. Synchrotron Rad.*, **2016**, *23(1)*, 369-373.
[40] Z. Otwinowski and W. Minor, Processing of X-ray diffraction data collected in oscillation mode, in *Methods in Enzymology*, Academic Press, **1997**, *276*, 307-326.
[41] G. M. Sheldrick, *Acta Cryst.*, **2015**, *A71*, 3-8.
[42] G. M. Sheldrick, *Acta Cryst.*, **2015**, *C71*, 3-8.
[43] O. V. Dolomanov, L. J. Bourhis, R. J. Gildea, J. A. K. Howard and H. Puschmann, *J. Appl. Crystallogr.*, **2009**, *42(2)*, 339-341.
[44] P. V. D. Sluis and A. L. Spek, *Acta Cryst.*, **1990**, *A46*, 194-201.
[45] A. L. Spek, *Acta Cryst.*, **2015**, *C71*, 9-18.
[46] H. Seong, M. Choi, S. Park, H. Kim, J. Kim, W. Kim, J. S. Yoo and D. Lee, *ACS Energy Lett.*, **2022**, *7(12)*, 4177-4184.
[47] J. Ge, H.-B. Yao, W. Hu, X.-F. Yu, Y.-X. Yan, L.-B. Mao, H.-H. Li, S.-S. Li and S.-H. Yu, *Nano Energy*, **2013**, *2(4)*, 505-513.
[48] X. Du, Z. Chen, Z. Li, H. Hao, Q. Zeng, C. Dong and B. Yang, *Adv. Energy Mater.*, **2014**, *4(9)*, 1400135.
[49] G.-F. Li, D. Yang and P.-Y. A. Chuang, *ACS Catal.*, **2018**, *8(12)*, 11688-11698.
[50] Y. Zhu, W. Zhou, Y. Zhong, Y. Bu, X. Chen, Q. Zhong, M. Liu and Z. Shao, *Adv. Energy Mater.*, **2017**, *7(8)*, 1602122.
[51] Z. Song, K. Wang, Q. Sun, L. Zhang, J. Li, D. Li, P.-W. Sze, Y. Liang, X. Sun, X.-Z. Fu and J.-L. Luo, *Adv. Sci.*, **2021**, *8(14)*, 2100498.
[52] W. Zhong, Z. Lin, S. Feng, D. Wang, S. Shen, Q. Zhang, L. Gu, Z. Wang and B. Fang, *Nanoscale*, **2019**, *11*, 4407-4413.
[53] C. Hu, L. Zhang and J. Gong, *Energy Environ. Sci.*, **2019**, *12*, 2620-2645.
[54] S. Fletcher, *J. Solid State Electrochem.*, **2009**, *13*, 537-549.
[55] J. Jiang, F. Sun, S. Zhou, W. Hu, H. Zhang, J. Dong, Z. Jiang, J. Zhao, J. Li, W. Yan and M. Wang, *Nat. Commun.*, **2018**, *9*, 2885.
[56] H. Chen, P. Kannan, L. Guo, H. Chen and D.-H. Kim, *J. Mater. Chem.*, **2011**, *21*, 18271-18278.
[57] S. Ren, D. Joulié, D. Salvatore, K. Torbensen, M. Wang, M. Robert and C. P. Berlinguette, *Science*, **2019**, *365(6451)*, 367-369.
[58] W. H. Lee, Y.-J. Ko, Y. Choi, S. Y. Lee, C. H. Choi, Y. J. Hwang, B. K. Min, P. Strasser and H.-S. Oh, *Nano Energy*, **2020**, *76*, 105030.
[59] W. Ren, X. Tan, C. Jia, A. Krammer, Q. Sun, J. Qu, S. C. Smith, A. Schueler, X. Hu and C. Zhao, *Angew. Chem. Int. Ed.*, **2022**, *61(26)*, e202203335.
[60] X. Y. Zhang, W. J. Li, J. Chen, X. F. Wu, Y. W. Liu, F. Mao, H. Y. Yuan, M. Zhu, S. Dai, H. F. Wang, P. Hu, C. Sun, P. F. Liu and H. G. Yang, *Angew. Chem. Int. Ed.*, **2022**, *61(28)*, e202202298.